Tm^{3+} and Nd^{3+} singly doped $LiYF_4$ single crystals with 3−5 μm mid-infrared luminescence

Shanshan Li (李珊珊)[1], Peiyuan Wang (汪沛渊)[1], Haiping Xia (夏海平)[1*], Jiangtao Peng (彭江涛)[1], Lei Tang (唐 磊)[1], Yuepin Zhang (张约品)[1], and Haochuan Jiang (江浩川)[2]

[1]*Key Laboratory of Photoelectronic Materials, Ningbo University, Ningbo 315211, China*

[2]*Ningbo Institute of Materials Technology and Engineering, Chinese Academy of Sciences, Ningbo 315211, China*

[*]*Corresponding author: hpxcm@nbu.edu.cn*

Received October 30, 2013; accepted December 19, 2013; posted online January 27, 2014

Mid-infrared (MIR) emissions of 2.4 and 3.5 μm from Tm^{3+}:$LiYF_4$ single crystals attributed to $^3H_4 \rightarrow {}^3H_5$ and $^3H_5 \rightarrow {}^3F_4$ transitions as well as MIR emissions of 4.2, 4.3, and 4.5 μm from Nd^{3+}: $LiYF_4$ lasers attributed to $^4I_{15/2} \rightarrow {}^4I_{13/2}$, $^4I_{13/2} \rightarrow {}^4I_{11/2}$, and $^4I_{11/2} \rightarrow {}^4I_{9/2}$ transitions, respectively, are observed. $LiYF_4$ single crystals possess high transmittance of over 85% in the 2.5−6 μm range. The large emission cross-sections of Tm-doped crystals at 2.4 μm (1.9×10^{-20} cm^2) and Nd-doped crystals at 4.2 μm (0.84×10^{-20} cm^2) as well as the high rare-earth doping concentrations, excellent optical transmission, and chemical-physical properties of the resultant samples indicate that Nd^{3+} and Tm^{3+} singly doped crystals may be promising materials for application in MIR lasers.

OCIS codes: 160.3380, 160.4760, 160.5690, 140.3380.

doi: 10.3788/COL201412.021601.

The mid-infrared (MIR) spectral region in the 3−5 μm[1,2] range is of considerable interest in a large number of applications, such as in laser remote sensing of biochemical agents, gas sensors, infrared (IR) countermeasures, medical diagnostics, basic IR spectroscopy, and free-space communications. MIR light sources in the range of 3–5 μm may be generally obtained through four ways. Firstly, the sources may be generated by a MIR semiconductor laser made of antimonide bandgap semiconductor materials, such as AlGaAsSb, InGaAsSb, and InAs/(In)GaSb[3]. Secondly, MIR laser outputs may be achieved using nonlinear frequency conversion technology based on $ZnGeP_2$ and $AgGaSe_2$ crystals[4]. Thirdly, a shortwave IR source may be tuned to MIR levels using frequency conversion technology[5]. Finally, rare-earth doped glass fibers and crystals as well as transition metal doped II-VI semiconductor materials pumped by solid-state lasers can emit wavelengths between 3 and 5 μm.

Despite the favorable outputs the aforementioned methods produce, however, each technique presents corresponding technical defects and limitations. Today, PbS/PbSe semiconductor lasers and quantum cascade lasers are the only commercially available MIR laser devices. Unfortunately, these devices cannot be applied in high-temperature cases because they mainly operate under low-temperature conditions. Researchers have recently begun to focus on rare-earth ion-doped glass and crystal IR light-emitting materials[6,7]. To achieve fluorescence emissions of approximately 3−5 μm in rare-earth ion-doped materials, the materials must possess low photon energies to minimize the phonon relaxation rate and improve the quantum efficiency of MIR transitions. The material itself must also have good transmission characteristics in the MIR region so that rare-earth ions doped in the host matrix can be excited to higher energy levels.

Although rare earth ion-doped chalcogenide glass has potential use in applications requiring 3–5 μm outputs, few studies discuss outputs in this range because of difficulties associated with achieving such wavelengths. Firstly, low rare-earth ion concentrations mean that rare earth ion-doped chalcogenide glass absorbs the energy of the pump source with poor efficiency, which hinders the observation of IR fluorescence phenomena. Secondly, concentration quenching of the dopants and impurities (e.g., -OH, -SH, etc.) in chalcogenide glass promotes nonradiative relaxation. Nonradiative relaxation is a resonant process that inhibits MIR fluorescence. Finally, chalcogenide glass has poor mechanical and thermal properties; thus, the glass is an unfavorable matrix for MIR applications.

$LiYF_4$ single crystals have been demonstrated to be excellent materials for laser matrices. Trivalent rare-earth elements have ionic radii similar to that of Y^{3+} in $LiYF_4$ single crystals. Rare-earth ion dopants introduced to such crystals can substitute Y^{3+} sites, which suggests that we can get a higher concentration rare earth doped $LiYF_4$ single crystal than the chalcogenide glass and that these crystals can absorb the pump energy fairly effectively. To produce $LiYF_4$ single crystals, the starting chemicals are usually of high purity and treated with anhydrous HF at 800 °C for 8–10 h to ensure the complete removal of residual moisture in the fluorides. $LiYF_4$ single crystals have high transmittance in the 3–5 μm range and surpass chalcogenide glass in terms of chemical durability and thermal stability. Thus, studies on MIR lasers can be extended beyond the limitations of chalcogenide glasses. Rare earth ion-doped $LiYF_4$ single crystals may present a promising material for application in 3–5 μm MIR light sources.

In this MIR, a modified Bridgman process is applied to grow Tm- and Nd-doped $LiYF_4$ crystals. The 3–5 μm MIR spectroscopic properties of $LiYF_4$ crystals doped

with $Tm^{3+}$and Nd^{3+} are observed during pumping at 808 nm, and the fluorescence emission cross-sections of peaks in the MIR region were calculated using the Futchbauer-Ladenburg (FL) equation.

Crystals with molar compositions of 51.5LiF-47.5YF_3-1Re (Re=TmF_3, NdF_3) were prepared and ground adequately for 1 h in a mortar. The mixtures were then sintered with anhydrous HF at 800 °C for 8−10 h to convert the feed material into polycrystalline bars and complete remove moisture and oxygen impurities in the fluoride powder[8]. The temperature gradient of the solid-liquid interface, which is an important parameter in crystal synthesis, was controlled to 50–60 °C/cm during the fabrication of the crystals. Details of the crystal growth process are described in Refs. [9−11].

Typical crystals grown by the Bridgman method are shown in Fig. 1. Small pale opaque matter of about several centimeters in length is observed at the top of the crystals, corresponding to the final portion of the melt to freeze, which may be attributed to excess LiF in the starting materials. The grown crystal was cut into small pieces along the growth orientation and polished to approximately 2.5-mm thickness for optical measurements.

The structure of the crystals was investigated by X-ray diffractometry (XRD) using an XD-98X diffractometer (XD-3, Beijing, China). The absorption spectrum was recorded by a U-4100UV/VIS/NIR spectrophotometer. The excitation beam was obtained from an 808 nm LD. Fluorescence was recorded by a Triax320 fluorescence spectrometer, in which InAs and PbSe detectors were respectively used for the 2.0–3.0 and 3.0–5.0 μm ranges. All of the measurements were conducted at room temperature.

The XRD patterns of the as-grown Tm^{3+}- and Nd^{3+}-doped crystals along with the standard line pattern of orthorhombic-phase $LiYF_4$ (JCPD Card No. 77-0816) are shown in Fig. 2. By comparing the peak positions of $LiYF_4$ with those in JCPD 77-0816, the current doping level may be concluded to cause no obvious peak shifts or secondary phases.

Figure 3 shows the absorption spectra and absorption

Fig. 1. (Color online) Images of the Tm^{3+}: $LiYF_4$ and Nd^{3+}: $LiYF_4$ single crystals.

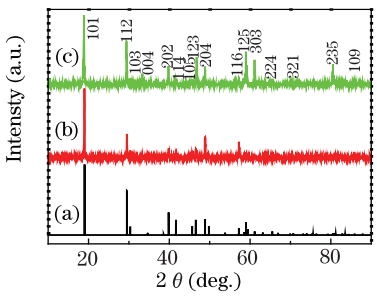

Fig. 2. (Color online) (a) Standard line pattern of orthorhombic-phase $LiYF_4$ (JCPD Card No. 77-0816), (b) XRD pattern of Tm^{3+}: $LiYF_4$ single crystals, and (c) XRD pattern of Nd^{3+}: $LiYF_4$ single crystals.

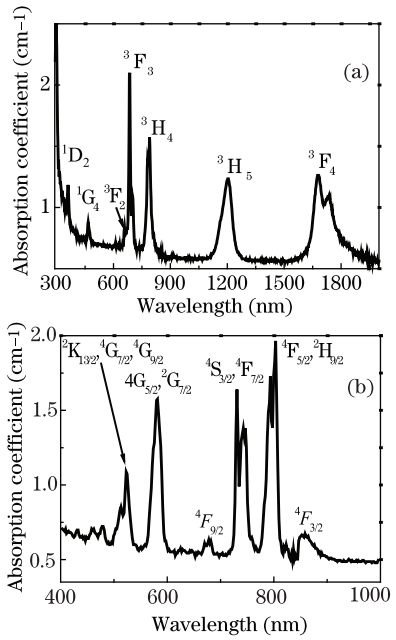

Fig. 3. Absorption spectra of (a) Tm^{3+}:$LiYF_4$ and (b) Nd^{3+}:$LiYF_4$ single crystals.

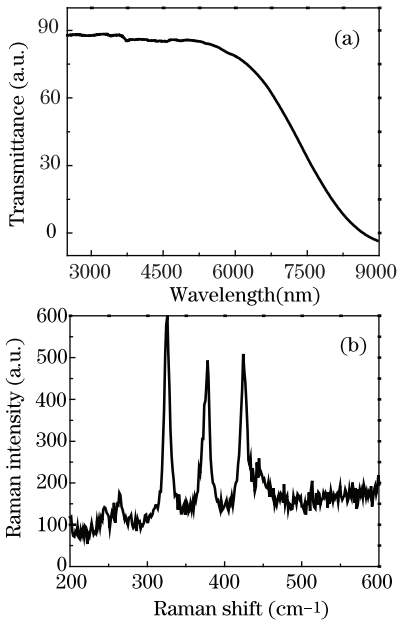

Fig. 4. (a) IR transmittance spectrum and (b) Raman spectrum of $LiYF_4$ single crystals.

coefficients of Tm^{3+}- and Nd^{3+}-doped $LiYF_4$ single crystals. Absorption bands are labeled for Tm^{3+} and Nd^{3+} ions corresponding to transitions from the ground state to upper states.

Figure 4(a) presents the IR transmittance spectrum of $LiYF_4$ single crystals. The maximum transmittance is as high as 89%, which suggests that oxide and oxyfluoride compounds are nearly absent in the crystals. High transmittance is observed at wavelengths of 2700–6000 nm. The emission intensity of rare-earth ions may be reduced significantly by residual OH^-[10]. Thus, the excellent IR transmittance property of $LiYF_4$ single crystals allows their potential application as MIR laser materials without such OH^- caused absorption. Figure 4(b)

displays the Raman spectrum of $LiYF_4$ single crystals. $LiYF_4$ single crystals clearly have very low phonon energy. The maximum phonon energy is approximately 425 cm^{-1}, which indicates that $LiYF_4$ may be used as a potential material for MIR emissions.

The MIR emission spectrum of Tm^{3+}:$LiYF_4$ single crystals is shown in Fig. 5(a). The emission bands at 2.4 and 3.5 μm in Fig. 5(a) are ascribed to $^3H_4 \rightarrow ^3H_5$ and $^3H_5 \rightarrow ^3F_4$ transitions, respectively. Figure 5(b) shows the energy level of Tm^{3+} and energy transfer mechanism when the sample is excited by an energy of 808 nm.

Figure 6(a) shows the MIR emissions of Nd^{3+}:$LiYF_4$ single crystals. Three emission bands are observed at 4.2, 4.3, and 4.5 μm, corresponding to the transitions of $^4I_{15/2} \rightarrow ^4I_{13/2}$, $^4I_{13/2} \rightarrow ^4I_{11/2}$, and $^4I_{11/2} \rightarrow ^4I_{9/2}$, respectively. Figure 6(b) shows the energy-transfer mechanism of Nd^{3+}.

The emission cross-sections were calculated using the FL equation provided in Ref. [12]:

$$\sigma_{\rm em}(\lambda) = \frac{\lambda^5 \cdot I(\lambda)}{8\pi n^2 \tau_{\rm rad} \int \lambda I(\lambda) {\rm d}\lambda}, \quad (1)$$

where $I(\lambda)$ is the intensity of the corrected emission spectrum, $\tau_{\rm rad}$ is the radiative lifetime, c is the velocity of light, and n is the refractive index of the crystals (1.4466), as taken from Ref. [13]. The calculated emission cross-sections are summarized in Table 1.

In conclusion, Tm^{3+}- and Nd^{3+}-doped $LiYF_4$ single crystals are prepared using the Bridgman method. $LiYF_4$ single crystals show high transmittance of over 85% at MIR wavelengths ranging from 2.5 to 6 μm and a low maximum phonon energy of approximately 425 cm^{-1}. MIR emissions of 3.5 μm from Tm^{3+}: $LiYF_4$ are attributed to $^3H_5 \rightarrow ^3F_4$ transitions, while MIR emissions of 4.2, 4.3, and 4.5 μm from Nd^{3+}: $LiYF_4$ single crystals

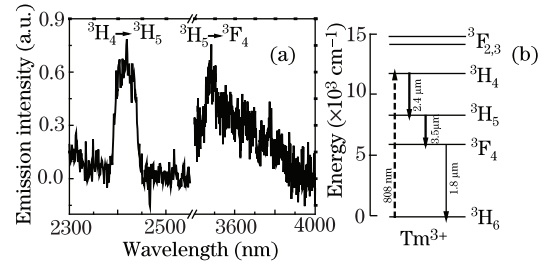

Fig. 5. (a) MIR emission spectrum of Tm^{3+}:$LiYF_4$ single crystals and (b) energy transfer mechanism of Tm^{3+}.

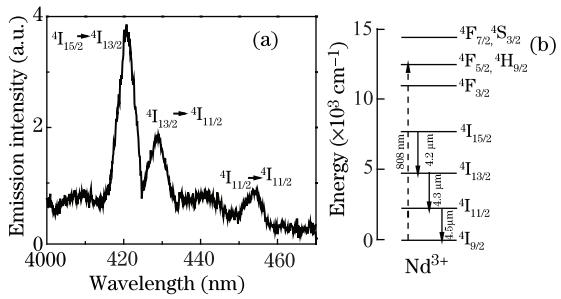

Fig. 6. (a) MIR emission spectrum of Nd^{3+}: $LiYF_4$ single crystals and (b) energy transfer mechanism of Nd^{3+}.

Table 1. Emission Wavelengths, Peak Cross-sections, and Radiative Lifetimes of MIR Transitions of Tm^{3+}- and Nd^{3+}-doped $LiYF_4$ Single Crystals

Rare-earth Transition	λ (peak) (μm)	$\tau_{\rm rad}$ (ms)	$\sigma_{\rm em}$ ($\times 10^{-20}$ cm ^{2})
Tm^{3+}:$^3H_4 \rightarrow ^3H_5$	2.4	0.22[14]	1.96
Tm^{3+}:$^3H_5 \rightarrow ^3F_4$	3.5	0.92[14]	0.91
Nd^{3+}:$^4I_{15/2} \rightarrow ^4I_{13/2}$	4.2	5.40[15]	0.84
Nd^{3+}:$^4I_{13/2} \rightarrow ^4I_{11/2}$	4.3	7.19[15]	0.64
Nd^{3+}:$^4I_{11/2} \rightarrow ^4I_{9/2}$	4.5	21.7[15]	0.33

are respectively attributed to $^4I_{15/2} \rightarrow ^4I_{13/2}$, $^4I_{13/2} \rightarrow ^4I_{11/2}$, and $^4I_{11/2} \rightarrow ^4I_{9/2}$ transitions. These emissions are observed under LD excitation of 808 nm. The crystals feature high rare earth element-doping concentrations and excellent chemical-physical properties; thus, these crystals have great application potential in 3–5 μm mid-emission lasers.

This work was supported by the National Natural Science Foundation of China (Nos. 51272109 and 50972061), the Natural Science Foundation of Zhejiang Province (No. R4100364), the Natural Science Foundation of Ningbo City (No. 2012A610115), and the K. C. Wong Magna Fund in Ningbo University.

References

1. H. Wu, L. Wang, F. Liu, H. Peng, J. Zhang, C. Tong, Y. Ning, and L. Wang, Chin. Opt. Lett. **11,** 091401 (2013).
2. E. Kasper, M. Kittler, M. Oehme, and T. Arguirov, Photon. Res. **1,** 69 (2013).
3. A. Joullie and P. Christol, Comptes Rendus Physique **4,** 621 (2003).
4. X. Shu, T. Liu, G. Zhang, X. Chen, J. Qin, and C. Chen, Chin. J. Inorg. Chem. **22,** 1163 (2006).
5. B. Yao, Y. Wang, and Q. Wang, Laser Technol. (in Chinese) **26,** 217 (2002).
6. F. Charpentier, F. Starecki, J. L. Doualan, P. Jovari, P. Camy, J. Troles, S. Belin, B. Bureau, and V. Nazabal, Mater. Lett. **101,** 21 (2013).
7. E. Virey, M. Couchaud, C. Faure, B. Ferrand, C. Wyon, and C. Borel, J. Alloys and Compd. **275,** 311 (1998).
8. H. Chen, S. Fan, H. Xia, and J. Xu, Mater. Sci. Lett. **21,** 457 (2002).
9. J. Hu, H. Xia, H. Hu, Y. Zhang, and H. Jiang, J. Appl. Phys. **112,** 073518 (2012).
10. L. Tang, H. Xia, P. Wang, J. Peng, Y. Zhang, H. Jiang, and H. Chen, Mater. Lett. **104,** 37 (2013).
11. L. Tang, H. Xia, P. Wang, J. Peng, and H. Jiang, Chin. Opt. Lett. **11,** 061603 (2013).
12. I. Sokolska, E. Heumann, S. Kuch, and T. Lukasiewicz, Appl. Phys. B **71,** 893 (2000).
13. X. Yu, H. Chen, S. Wang, Y. Zhou, A. Wu, and S. Dai, J Inorg. Mater. **26,** 923 (2011).
14. S. Dai, B. Peng, P. Zhang, T. Xu, X. Wang, Q. Nie, and X. Zhang, J. Non-Cryst. Solids. **356,** 2424 (2010).
15. M. Ichikawa, Y. Ishikawa, T. Wakasugi, and K. Kadono, Opt. Mater. **35,** 1941 (2013).